Spatial analysis of the ancient proteome of archeological teeth using mass spectrometry imaging

Dekker, J.; Larson, T.; Tzvetkov, J.; Harvey, V.L.; Dowle, A.; Hagan, R.; ... ; Hendy, J.

Received: 13 November 2022 | Revised: 28 January 2023 | Accepted: 29 January 2023

DOI: 10.1002/rcm.9486

RESEARCH ARTICLE

Rapid Communications in Mass Spectrometry WILEY

Spatial analysis of the ancient proteome of archeological teeth using mass spectrometry imaging

Joannes Dekker[1,2,3] | Tony Larson[4] | Jordan Tzvetkov[5] | Virginia L. Harvey[1,6] | Adam Dowle[4] | Richard Hagan[1] | Paul Genever[5] | Sarah Schrader[3] | Marie Soressi[3] | Jessica Hendy[1]

[1]BioArCh, Department of Archaeology, University of York, York, UK

[2]Section for GeoBiology, Globe Institute, University of Copenhagen, Copenhagen, Denmark

[3]Faculty of Archaeology, Leiden University, Leiden, the Netherlands

[4]Metabolomics & Proteomics Laboratory, Bioscience Technology Facility, Department of Biology, University of York, York, UK

[5]Department of Biology, University of York, York, UK

[6]Department of Biological Sciences, University of Chester, Chester, UK

Correspondence
Joannes Dekker, BioArCh, Department of Archaeology, University of York, York, UK.
Email: jan@palaeome.org

Funding information
Leverhulme Trust, Grant/Award Number: Philip Leverhulme Prize; Nederlandse Organisatie voor Wetenschappelijk Onderzoek, Grant/Award Numbers: Neanderthal Legacy, VI.C.191.07; University of York, Grant/Award Number: Research Priming Fund

Rationale: Proteins extracted from archaeological bone and teeth are utilised for investigating the phylogeny of extinct and extant species, the biological sex and age of past individuals, as well as ancient health and physiology. However, variable preservation of proteins in archaeological materials represents a major challenge.

Methods: To better understand the spatial distribution of ancient proteins preserved within teeth, we applied matrix assisted laser desorption/ionisation mass spectrometry imaging (MALDI-MSI) for the first time to bioarchaeological samples to visualise the intensity of proteins in archaeological teeth thin sections. We specifically explored the spatial distribution of four proteins (collagen type I, of which the chains alpha-1 and alpha-2, alpha-2-HS-glycoprotein, haemoglobin subunit alpha and myosin light polypeptide 6).

Results: We successfully identified ancient proteins in archaeological teeth thin sections using mass spectrometry imaging. The data are available via ProteomeXchange with identifier PXD038114. However, we observed that peptides did not always follow our hypotheses for their spatial distribution, with distinct differences observed in the spatial distribution of several proteins, and occasionally between peptides of the same protein.

Conclusions: While it remains unclear what causes these differences in protein intensity distribution within teeth, as revealed by MALDI-MSI in this study, we have demonstrated that MALDI-MSI can be successfully applied to mineralised bioarchaeological tissues to detect ancient peptides. In future applications, this technique could be particularly fruitful not just for understanding the preservation of proteins in a range of archaeological materials, but making informed decisions on sampling strategies and the targeting of key proteins of archaeological and biological interest.

1 | INTRODUCTION

Proteins extracted from archaeological teeth are used for a wealth of applications, including identifying the phylogeny of extinct[1–4] and extant species,[5–7] biological age estimation[8] and biological sex identification.[9] In addition, the pulp chamber has also been targeted as a source of proteins associated with pathogens.[10] Other archaeological science approaches, such as carbon and nitrogen isotope analysis and radiocarbon dating of bone collagen, depend on the preservation of bone proteins.[11]

Variation in the preservation and distribution of proteins in archaeological material is a substantial challenge for the consistency and applicability of palaeoproteomics, with biological and diagenetic processes leading to differences in the abundance and presence of proteins between samples.[8,12,13] While there is a substantial body of work on protein diagenesis in archaeological bones and teeth,[14] our knowledge of the spatial distribution of proteins within these archaeological tissues remains limited. Understanding this distribution would contribute to tackling several challenges in palaeoproteomics: the identification of specific target locations for sampling (and, as a consequence, minimising unnecessary damage), the interpretation of data from sequential sampling in dental tissue and the variable preservation of particular proteins in archaeological materials. To address these challenges, we aimed to spatially explore the distribution of proteins in archaeological teeth using matrix-assisted laser desorption ionisation mass spectrometry imaging (MALDI-MSI). For the first time we explored the usefulness of using MALDI-MSI for understanding the distribution and preservation of proteins in bioarchaeological remains, here focusing on dental tissues.

1.1 | The distribution of proteins in teeth

Teeth contain three dominant mineralised tissue-types, enamel, dentine and cementum, as well as soft tissue of the dental pulp, the latter of which rarely preserves in archaeological contexts. These tissue types contain distinct proteomes, reflecting their formation and biological functions.[15–17] For example, the protein amelogenin, responsible for the growth of hydroxyapatite crystals, is dominant in enamel tissue, while the proteome of dentine is dominant in collagenous proteins. Systematic differences in proteome composition also occur in the different stages of tooth mineral development and between the tooth types, such as molars and canines,[18–20] for example distinct proteomes have been observed in deciduous versus permanent dental cementum.[21]

Spatial patterns in the proteome within teeth tissue types have also been explored in archaeological and modern tissues using a variety of methods. For example, Hirano et al.[22] employed MSI to show that several compounds show distinct spatial patterns within teeth, which allowed distinguishing dentine, enamel and the dental pulp cavity, although it was not possible to identify the specific proteins generating those signals. Within dentine alone, Procopio et al.[8] demonstrated differences in the proteome between the top, middle and root dentine by comparing a series of liquid chromatography tandem mass spectrometry (LC–MS/MS) samples. Czermak et al.[23] used fluorescence to examine the spatial distribution of proteins in dentine affected by caries, observing that areas of degraded collagen could be detected using fluorescence imaging. They argue that even from some of these degraded areas unaltered collagen can still be recovered, although larger samples are required. Focusing on human enamel, Mitsiadis et al.[24] used antibody staining to observe that the distribution of the protein amelogenin resembles a zebra-like pattern of alternating high- and low-abundance layers.[24]

1.2 | Sequential sampling of archaeological proteins in dental tissues

In archaeological contexts, the spatial distribution of proteins due to dental growth is utilised in the isotope analysis of sequentially sampled dentine, an important approach in palaeodietary studies.[25–27] This approach exploits the fact that teeth grow incrementally with biological age until they are fully developed[28] and therefore the isotope composition of constituent proteins in these increments reflects diet in relatively narrow time windows.[29] For example, stable isotopes analysis of $\delta^{18}O$ and $\delta^{13}C$ in mammal teeth demonstrates seasonal patterns of diet,[30] and by strategic sequential sampling of multiple teeth in humans it is possible to reconstruct dietary changes through infancy, childhood and adolescence.[31] Correlation of spatial changes in isotope ratios with linear enamel hypoplasia, a morphological stress marker,[32] has also been attempted, although no significant correlation was found.[33]

Intra-tooth sequential sampling (microsampling) involves sectioning a tooth and excising small chunks of tooth (0.5–1.25 mm in width).[28,34–37] However, the standard sampling method of cutting transverse sections from crown to root for sequential sampling does not directly follow the direction of growth and the resulting microsamples will consist of multiple growth increments, which reduce the temporal resolution of the sample.[36] There have been developments to improve the temporal resolution of microsamples, such as comparing small punches on the outer layer of dentine versus microslices of dentine.[38] Despite the value of this approach, it remains unclear how the potential spatial distribution of protein in teeth would affect sequential stable isotope analysis and if microsamples would contain a consistently representative proteome. Additionally, not all tissues are suitable for microsampling due to the size and composition of the sample, for example primarily due to its small size it is not current practice to perform sequential proteomic analysis of dental calculus. Moreover, having a greater understanding of the spatial distribution of the target proteins of interest could be used to prevent unnecessary destructive sampling and would allow informed decisions to be made regarding sampling particular areas within a tissue.

1.3 | Mass spectrometry imaging

In this study we explore mass spectrometry imaging (MSI) as a potential method to identify and study intratissue variation in archaeological samples. MSI acts like a 'chemical microscope', where molecules are desorbed or extracted across a 2D surface and then directly analysed using mass spectrometry, enabling a visualisation of the spatial distribution of compounds of interest. In matrix assisted laser desorption/ionisation - time of flight mass spectrometry (MALDI-TOF MS), an approach often used for zooarchaeology by mass spectrometry (ZooMS), mass spectra are acquired via the ablation and ionisation of extracted peptides on a steel plate. In contrast, MALDI-MSI utilises a flat sample surface (typically created using thin sectioning). The sample's surface is divided into a raster and a mass spectrum acquired for each pixel. By selecting target masses of interest, the result is an image of the intensity of that mass distributed across the sample surface. The pixel size determines image resolution, with smaller pixels yielding more detailed spatial distribution for each mass measured, but also increasing the time and cost of analysis.

MALDI-MSI has seen wide applicability in the biological and medical sciences, particularly in understanding the location of particular target pharmaceutical and biological compounds, such as disease biomarkers,[39–42] even in single cells.[43,44] For mineralised tissues, MSI has seen fewer applications owing to the lack of sample preparation protocols suitable for hard tissues. However, MSI has been successfully applied to modern mouse bone and teeth,[45] rat bone,[46] chicken bone[47] and human teeth.[22] MSI on bone has been used to understand protein expression in bone tumours, with visualisation using MALDI-MSI performed in tandem with in vivo histology,[48] the visualisation of bone lipids[49] and the detection of the drug methadone in bone tissues.[46]

Due to the rareness of MSI being used on samples from hard tissues, MALDI-MSI has rarely been applied to archaeological or palaeontological contexts. Kramell et al.[50] utilised MALDI-MSI to detect dyes on a fabric fragment dating to 2nd century BC–5th century AD in the Tarim Basin, China. An alternative form of mass spectrometry imaging called secondary ion mass spectrometry (SIMS), together with a time of flight and an Orbitrap mass analyzer, has been used more frequently. SIMS has mainly been applied to different types of archaeological remains for the visualisation of the spatial distribution of proteins and lipids, such as ceramic vessels,[51] paintings[52,53] and patina on wooden statuettes.[54] However, SIMS has decreased sensitivity[55] and employs a harder ionisation compared to MSI, leading to further fragmentation of the already fragmented archaeological proteins, as well as a narrower mass range.[56,57] Especially for the analysis of archaeological remains, where diagenesis will already have fragmented any surviving proteins, these differences may be persuasive arguments for preferring MSI.

Although approximately 813 proteins have been identified in dentine,[58] it is not possible to detect and verify all these proteins by MALDI-MSI. To aid visualisation and interpretation, in this study we have focused our analysis on four biologically meaningful proteins, but the supplementary data included with this article could be used to study other proteins in dental tissues as well. The particular proteins investigated in this study are collagen type I alpha-1 and alpha-2, alpha-2-HS-glycoprotein, haemoglobin subunit alpha and myosin light polypeptide 6. These proteins were selected due to their archaeological relevance in previous applications, and to investigate the spatial distribution of proteins both associated and not associated with the bone mineral. Collagen is the most abundant protein in bone, and in archaeological contexts is frequently used to taxonomically identify bone or teeth fragments in addition to stable isotope analysis and radiocarbon dating. Alpha-2-HS-glycoprotein (fetuin-a) was selected as it has been suggested as a marker for biological age-at-death.[8] Haemoglobin subunit alpha is a common blood protein and was selected to visualise the presence of blood in the teeth. Lastly, myosin light peptide 6 is primarily expressed in muscle tissues and similarly is not commonly associated with the bone proteome.

For our analyses we applied a combined MALDI-MSI and LC–MS/MS approach. A schematic overview of our approach can be seen in Figure 1. LC–MS/MS analysis was required due to the difficulty of validating peptide identifications with MSI. A peak observed at the same *m/z* (mass-to-charge ratio) as a peptide of interest does not necessarily mean that it is the correct peptide, as the *m/z* value could represent a number of isobaric compounds. Furthermore, since the data is acquired from a tissue thin section rather than a filtered protein homogenate, there could be nonproteinaceous material (including artefacts) distorting the signal. Therefore, to improve the confidence of our peptide identifications, it is necessary to combine the MSI analysis with an independent method of protein identification (in this case, LC–MS/MS analysis). The samples for LC–MS/MS analysis were taken from the root of each tooth to enable direct comparison between the LC–MS/MS and MSI data. A consequence of sampling the root is that this region only contains dentine and the LC–MS/MS analysis will not provide any enamel protein peptides for MSI visualisation.

2 | MATERIALS AND METHODS

2.1 | Sample information

This study analysed nine archaeological and four modern teeth (Table 1). The archaeological teeth originate from the graveyard of the Eusebius church in Arnhem, the Netherlands. The graveyard is an attritional assemblage consisting of 789 individuals and spans the medieval and postmedieval periods (ca. 1350–1829 AD).[59] To minimise potential variation in the sample set we selected individuals of osteologically estimated male young adult (18–35 years) individuals. Accepted osteological methods for sex and age estimation were employed.[60] We selected teeth without any pathological conditions present, and where possible preferred to minimise the variation in tooth type across our sample selection. In practice, this has translated to a preference for premolars. Additionally, we attempted to minimise the number of pathological conditions present

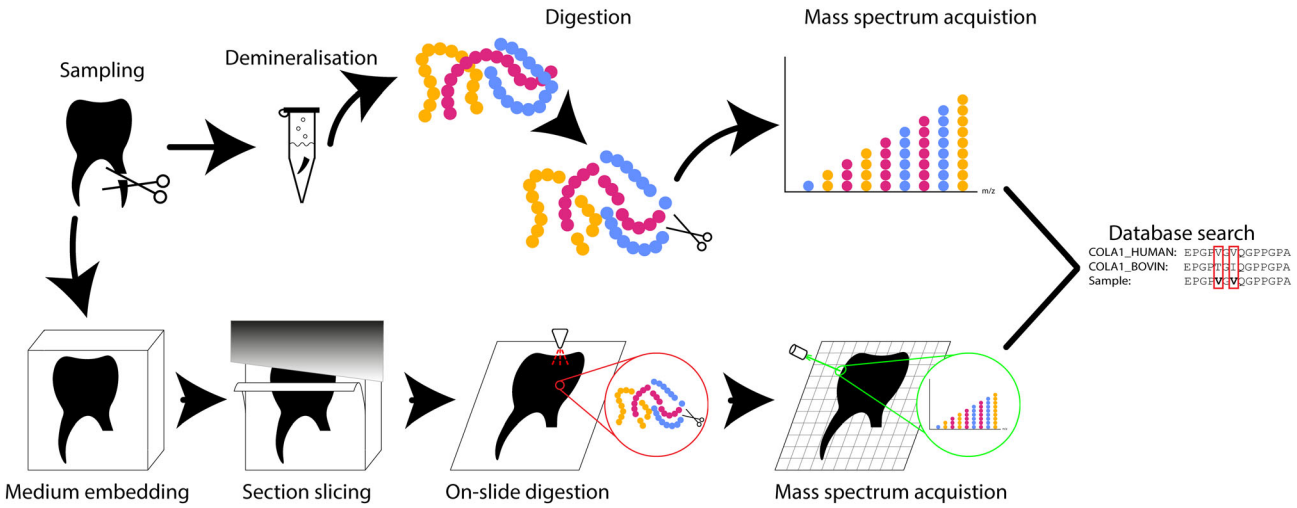

FIGURE 1 Schematic overview of the workflow in this study. A subsample was taken from each tooth, from which proteins were extracted and analysed using LC–MS/MS. The remainder of the whole tooth was sectioned and analysed using MALDI-MSI. The peaks selected for MSI visualisation were based on peptides identified by LC–MS/MS analysis [Color figure can be viewed at wileyonlinelibrary.com]

TABLE 1 Samples of archaeological and modern dental tissues utilised in this study

ID	Individual ID	Find ID	Skeletal element	LEH present on individual
Archaeological teeth				
1	302	126	Right maxillary second premolar	No
3	418	560	Right mandibular canine	Yes
4	531	636	Right mandibular second premolar	Yes
5	608	898	Right mandibular first premolar	Yes
6	663	926	Right mandibular canine	No
14	613	2,214	Left mandibular first premolar	Yes
15	716	2,340	Right mandibular first premolar	Yes
16	689	2,505	Right maxillary second incisor	Yes
17	310	550	Left mandibular first premolar	No
Modern teeth				
M1	n/a	n/a	Deciduous right maxillary second premolar	No
M7	n/a	n/a	Right maxillary second premolar	No
M8	n/a	n/a	Left maxillary second premolar	No
M13	n/a	n/a	Deciduous right maxillary second premolar	No

Abbreviations: ID, identification; LEH, linear enamel hypoplasia.

on the entire individual, with the exception of linear enamel hypoplasia (LEH) because of a hypothesised link between nonspecific stress and the abundance of particular proteins.[61] In this previous study no specific correlation between protein abundance and LEH was found, but this was to be expected as protein abundance was measured in samples from the femur and clavicle from adult individuals.[61] In our sample selection we tolerated the presence of LEH to investigate this effect of nonspecific stress on protein abundance in a more controlled manner. Furthermore, the time window in which LEH can form is relatively restricted[62] and thus it might enable us to observe potential differences in protein spatial patterns between individuals with and without LEH. LEH was present on six out of nine individuals analysed (Table 1).

Modern teeth were acquired from willing and informed participants who had healthy teeth removed by professional dentists for orthodontological (nonpathological) reasons. Informed consent for this analysis was granted and ethical approval for this research was granted by the University of York Department of Biology and Department of Archaeology Ethics Committee and in accordance with the UK Human Tissue Act (2004).

2.2 | Sample preparation (LC–MS/MS)

Peptides from archaeological and modern human teeth were extracted following Method 4 of Schroeter et al.[63] Two extraction blanks were also performed to monitor for laboratory-based contamination. Between 47.3 and 119.2 mg of tooth root were subsampled from teeth, then pulverised and demineralised in 1 ml of 0.6 M HCl at 4°C. After 48 h, samples were centrifuged, and the acid fraction was removed and stored at −20°C. The remaining pellets were washed three times with molecular-grade purified water. Neutralised pellets were then incubated overnight at 65°C in 500 µl of 50 mM ammonium bicarbonate. Samples were centrifuged for 10 min at 7200 ×*g* and the pellets were stored at −20°C. The remaining soluble protein was dried in a speed vacuum and 200 µg of protein weighed into a 1.5-ml Eppendorf tube, then 200 µl of 8 M urea was added to the weighed protein. Next, 20 µl was taken from this 200 µl of protein fraction and this subsampled fraction reduced by adding 2 µl of 100 mM dithiothreitol for 20 min at room temperature. Subsequently, 3 µl of 300 mM iodoacetamide was added for alkylation and samples left to react in the dark for 30 min. The extracted proteins were digested by adding 200 ng of trypsin (Promega) suspended in a solution of 135 µl of 100 mM ammonium bicarbonate and 1 µl of 1 M dithiothreitol and left to react at 37°C overnight. Digestion was stopped by adding 16 µl of 5% trifluoroacetic acid. Peptides were desalted using C18 ZipTips (Thermo Scientific) according to the manufacturer's protocol and peptides dried before LC–MS/MS analysis.

2.3 | LC–MS/MS data acquisition

Extracted peptides were loaded onto an mClass nanoflow ultra-performance liquid chromatography (UPLC) system (Waters) equipped with a nanoEaze M/Z Symmetry 100 Å C18, 5-µm trap column (180 µm × 20 mm; Waters) and a PepMap, 2-µm, 100 Å, C18 EasyNano nanocapillary column (75 µm × 500 mm; Thermo). As a first step of separation the peptides were washed from the trap column into the capillary column with 0.05% trifluoroacetic acid aqueous solvent at a flow rate of 15 µl/min. After 5 min it was assumed that all peptides had eluted so the flow was switched to the capillary column. In the capillary column a gradient between two solvents (A and B) was used to separate the peptides. Solvent A was an aqueous 0.1% formic acid (FA) solution, while solvent B consisted of 0.1% FA in acetonitrile (ACN). For the first 7 min the capillary column was washed with a solution consisting of solvent A and 3%–10% solvent B, with the concentration of solvent B increasing over time. After this the concentration of solvent B was steadily increased to 35% over the course of 30 min, then to 99% over 5 min and lastly the column was washed with a 99% concentration of solvent B for 4 min.

Separated peptides were introduced into an Orbitrap Fusion Tribrid mass spectrometer (Thermo Scientific) with an EasyNano ionisation source (Thermo Scientific). Xcalibur (version 4.0; Thermo Scientific) was used to acquire precursor (MS1) and fragment (MS2) mass spectra both in positive mode. The following instrument source settings were used: ion spray voltage 1900 V, sweep gas 0 Arb, ion transfer tube temperature 275°C. MS1 spectra were acquired in the Orbitrap with 120,000 resolution, scan range *m/z* 375–1500, automatic gain control (AGC) target value of 4e5 and maximum fill time 100 ms. Acquisition was data dependent and performed in topN mode selecting the 12 most intense precursors with charge states >1. Easy-IC was used for internal calibration. Dynamic exclusion was performed for 50 s post precursor selection and a minimum threshold for fragmentation was set at 5e3. MS2 spectra were acquired in the Orbitrap with 30 000 resolution, maximum fill time, 100 ms, higher energy collisional dissociation (HCD), and activation energy 32 normalised collision energy (NCE). The mass spectrometry proteomics data were deposited to the ProteomeXchange Consortium via the PRIDE[64] partner repository with the dataset identifiers PXD038114 and 10.6019/PXD038114.

2.4 | LC–MS/MS data analysis

Using MetaMorpheus (version 0.0.320) the spectral files were searched allowing for semi-tryptic protein cleavage against the Uniprot human proteome (UP000005640) and the in-built MetaMorpheus database of common contaminants, which includes the commonly used common repository of adventitious proteins (cRAP) database of common contaminants.[65,66] Before searching against these databases, MetaMorpheus performed a calibration and global post translational modification discovery (G-PTM-D) task, with common fixed and variable modifications included in the calibration task and common biological, common artefacts, metal and trypsin-digested modifications included in the G-PTM-D task. For successful identification a protein was required to have a *q* value of 0.01 and at least two distinct peptides. Any proteins identified in the two blanks were excluded from further analysis.

2.5 | Sample preparation (MALDI-MSI)

Tooth samples were processed for MSI following a protocol adapted from Fujino et al.[67] The teeth were demineralised for up to 3 weeks in 0.6 M HCl at 4°C, with the HCl being replaced with fresh reagent every 2 days. Demineralisation was halted when either the dentine became slightly pliable or there was a significant degree of enamel dissolution. No fixation treatment was applied to the teeth. Samples were neutralised with phosphate buffered saline (PBS) and incubated overnight with shaking at room temperature in a solution of 30% sucrose in PBS (Dulbecco A; Oxoid) for cryoprotection. The teeth were embedded in a 3% carboxymethylcellulose solution and rapidly frozen in a dry ice and ethanol mix. The frozen samples were stored at −80°C until cryosectioning. A cryostat (Bright) set to −24°C with a carbide steel blade and Superfrost Slides (Thermo Scientific) were used to produce 13-µm sections. Light scans of the thin sections can

be found in Figure S2. The thin sections were stored at −80°C before mass spectrometric analysis. Due to their size, some of the tooth thin sections (teeth 3, 4, 6 and 16) had to be acquired in two steps. The resulting raw files were combined during analysis, but this resulted in a black line being observed in the image.

Lipid removal and de-salting were performed by immersing the sections at room temperature for 1 min each in serial dilutions of 70% and 90% EtOH and finally for 10 s in 100% chloroform. Sections were air dried and uniformly covered with 12.5 µg/ml Trypsin (Promega) in 20 mM ammonium bicarbonate using an HTX-TM sprayer (Bruker). The following sprayer settings were used: 30°C spray nozzle temperature, 16 criss-cross passes and offset, 30 µl/min flow rate, 750 mm/min spray nozzle velocity, 2 mm track spacing, 10 psi nitrogen pressure, 3 L/min gas flow rate, 10 s drying time and nozzle height 40 mm. Tryptic digestion was facilitated by incubating overnight at 37°C in a humidity chamber. Following digestion, the sections were uniformly sprayed with 10 mg/ml α-Cyano-4-hydroxycinnamic acid matrix in 70% ACN using the same sprayer system, with settings adjusted to 75°C spray nozzle temperature, 12 passes, 120 µl/min flow rate, 1200 mm/min spray nozzle velocity, 3 mm track spacing, 10 psi nitrogen pressure, 3 L/min gas flow rate, 30 s drying time and nozzle height 40 mm.

2.6 | MSI data acquisition and analysis

Once the matrix had been applied, the samples were introduced to the Synapt G2 Si (Waters) mass spectrometer and analysed in positive ionisation on sensitivity mode. Red phosphorous was used for calibration, resulting in an root mean square mass error of <10 ppm. The acquisition area was set in Waters high-definition imaging (HDI) software to encompass the entire tooth and the pixel size was set to 50 × 50 µm. Mass spectra were acquired over a mass range of *m/z* 700–5000 and analysed in HDI with an *m/z* window of 0.04 Da. Following an exploratory investigation of the resulting mass spectra, the files were reprocessed using a target list based on the peaks identified in sample 16. The reprocessing removes intersample variation in the peak bins, thus allowing for a more direct comparison between samples. Sample 16 was chosen as the basis of the target list because it is one of the more complete and high-quality sections. The resulting image files were normalised using BASIS, an open source python script,[68] which consists of a mass correction and intrasample normalisation step. An inter-sample normalisation step was also applied to all samples, save for sample 14. Sample 14 had to be excluded because it was acquired as a pilot sample at a different resolution (100 × 100 µm). In this study we have interpreting peptide quantification from MSI data due to the lack of a suitable internal standard.

Target ions for visualisation were selected based on the LC–MS/MS data. First, the top five (if present) peptides with the highest intensity (as calculated by MetaMorpheus) across all samples combined were selected. A brief survey was then performed to check whether the MSI signal at these *m/z* values appeared to be endogenous, that is, there was a clear distinction in intensity between the matrix and the tooth tissue. Only peptides that provided a clear endogenous signal were included in further analysis. We observed that no clear endogenous signal could be observed for any peptide with an *m/z* higher than roughly 2000. In general, the lower the *m/z*, the clearer the MSI signal. Furthermore, to confirm that the target peptide is unique to a particular protein, the tryptic peptide analysis function of Unipept was used.[69] All selected peptide targets are uniquely found in only one human protein. The selected target peptides are listed in Table 2. The abundance of the selected peptide was visualised across the thin section according to a linear scale of the intensity of the given peptide for each pixel.

TABLE 2 Proteins and peptide masses targeted in this study for their spatial distribution in archaeological teeth

Uniprot ID	Protein name	Archaeological application	Example archaeological studies	Peptide target (M + H) (*m/z*)	Peptide amino acid sequence
P02452	Collagen alpha-1 (I) chain	Taxonomic identification	e.g., Buckley et al.[70]	898.51	GVVGLPGQR
				1105.58	GVQGPPGPAGPR
				1240.68	GVVGLPGQRGER
P08123	Collagen alpha-2 (I) chain	Taxonomic identification		1253.65	GLPGSPGNIGPAGK
				1267.68	GIPGPVGAAGATGAR
				1580.77	GPPGESGAAGPTGPIGSR
P02765	Alpha-2-HS-glycoprotein	Biological age-at-death marker	e.g., Procopio et al.,[13] Wadsworth and Buckley,[71] Sawafuji et al.[72]	802.36	QYGFCK
				1226.68	LDGKFSVVYAK
P69905	Haemoglobin subunit alpha	Blood protein	e.g., Solazzo et al.[73]	1529.74	VGAHAGEYGAEALER
				1660.78	VGAHAGEYGAEALERM
P60660	Myosin light polypeptide 6	Muscle protein	e.g., Solazzo et al.[73]	995.59	HVLVTLGEK
				1354.73	ALGQNPTNAEVLK
				1531.61	CDFTEDQTAEFK

3 | RESULTS

3.1 | Protein identification

Eighty-one distinct proteins were identified in archaeological and modern teeth, with the archaeological teeth containing on average 15 proteins, while the modern samples yielded an average of 45. The full list of protein identifications per sample is given in Table S1. As expected, collagen alpha-1 (I) chain (P02452) and collagen alpha-2 (I) chain (P08123) were highly abundant. Biologically, one would expect collagen alpha-1 (I) and alpha-2 (I) to occur in a ratio of 2:1. In our samples the ratio of the intensity of collagen alpha-1 (I) to alpha-2 (I) was on average 1.76 ± 0.15. Other frequently detected proteins were alpha-2-HS-glycoprotein (P02765), matrix Gla protein (P08493), biglycan (P21810), albumin (P02768), lumican (P51884) and periostin (Q15063). Osteocalcin (P02818), the most abundant noncollagenous protein in bone,[74,75] was only detected in three teeth (two archaeological, one modern) by LC–MS/MS.

3.2 | MSI analysis

First, we examined the distribution of peptides from the same protein within the same tooth section (Figure 2), unexpectedly finding that peptides from the same protein often, but not consistently, followed the same spatial patterns. Figure 2 presents the distribution of the three selected collagen alpha-1 (I) peptides (Table 2) for three archaeological teeth (6, 15 and 16) and an overview of the distribution of all selected peptides across all samples can be seen in Figure S1. An endogenous signal of collagen alpha-1 (I) peptides is observed because the intensity of peptides is low in the surrounding matrix. It is also observed that there is typically heterogeneous distribution of collagen alpha-1 (I) peptides within the tooth, with 'hot spots' of peptide intensity (Figures 2 and 3). Moreover, in a few teeth collagen alpha-1 (I) peptides do not show consistent spatial distribution patterns within the same tooth. For example, while in two teeth (6 and 16) collagen peptides show similar distribution patterns, although with different intensities, the spatial distributions of collagen alpha-1 (I) peptides in tooth 15 are variable (Figure 2). For example, *m/z* 898.42 seems to have three areas of high intensity along the tooth's edge, mainly focused around the top of the crown. In contrast, the *m/z* 1105.51 peptide has one large area of high intensity right in the centre of the tooth. This variation in spatial patterning within the same tooth was even more pronounced in collagen alpha-2 (I) (Figure 3). Whereas for collagen alpha-1 (I) the intratooth variation in spatial distribution between peptides of the protein was restricted to a few teeth, all teeth showed clear intratooth differences in collagen alpha-2 (I) peptide distribution. In general, the peptides at *m/z* 1253.58 and *m/z* 1580.74 appear similar within the same tooth, while the peptide at *m/z* 1267.59 deviates from this pattern (but see also samples 5, 14 and M13; Figure S1).

Similarly, we also observe spatial variation of peptides from the same protein between different teeth (Figure 2). For example, the collagen alpha-1 (I) peptide *m/z* 898.42 is not homogeneously distributed within teeth 6 or 16 and the spatial distribution between the two teeth (the inter-tooth variation) also differs. Although teeth 6 and 16 are displayed with the same orientation, in sample 16 a 'hotspot' can be observed on the lingual side just above the tip of the root, whilst the same peptide in sample 6 shows a concentration towards the very end of the root.

We also examined the differences in spatial distribution in the peptides of our other target proteins in all teeth (Figure S1) and found that for alpha-2-HS-glycoprotein, haemoglobin subunit alpha and overall myosin light polypeptide 6 for most teeth there was little to no variation in spatial pattern of the target peptides of the same protein within the same tooth. An exception is tooth 15, which showed clear differences in peptide spatial distribution for alpha-2-HS-glycoprotein and myosin light polypeptide 6.

We also compared the spatial distribution of different proteins in the same tooth section, finding that there is some consistency in how different proteins are distributed within the tooth. Figure 4 displays the distribution of one peptide from each of our target proteins from two teeth (6 and 16). Within the same tooth, alpha-2-HS-glycoprotein, myosin light polypeptide 6 and collagen alpha-1 (I) have similar spatial distributions. For example, in sample 16, alpha-2-HS-glycoprotein, myosin light polypeptide 6 and collagen alpha-1 (I) have a 'hot spot' on the lingual side near the tip of the root. However, the haemoglobin peptides display a relatively homogenous, but low intensity distribution. Surprisingly, peptides from collagen alpha-2 (I) (e.g., *m/z* 1267.59 as presented in Figure 4) do not follow the spatial distribution of collagen alpha-1 (I) within the same tooth. It would be expected that collagen alpha-1 (I) and alpha-2 (I) would show similar patterns of spatial distribution, given their association together in the collagen (I) triple helix.

4 | DISCUSSION

In this study ancient proteins from dental tissue were visualised using MSI, demonstrating that this technique holds promise for capturing the spatial distribution of proteins in archaeological samples. However, we observed that there is unexpected and inconsistent variation in the distribution of peptides from the same protein, and inconsistent variation in the distribution of different proteins within the same tooth, therefore some challenges remain for the application of MSI to bioarchaeological samples, particularly in the creation of dental thin sections and in the authentication of protein identification.

Considering the peptide distribution in all teeth, there were three main points that did not meet our expectations. First, we had expected the collagen alpha-1 (I) and alpha-2 (I) peptides to show similar spatial patterns. In humans, collagen type I takes the form of a triple helix, where two of the strands are contributed by collagen alpha-1 and the third by collagen alpha-2, and therefore as the two are part of the same larger molecule, their spatial patterns should be similar. Furthermore, the collagen distribution in teeth visualised using fluorescence and immunochemical chemiluminescence[12,23] also did

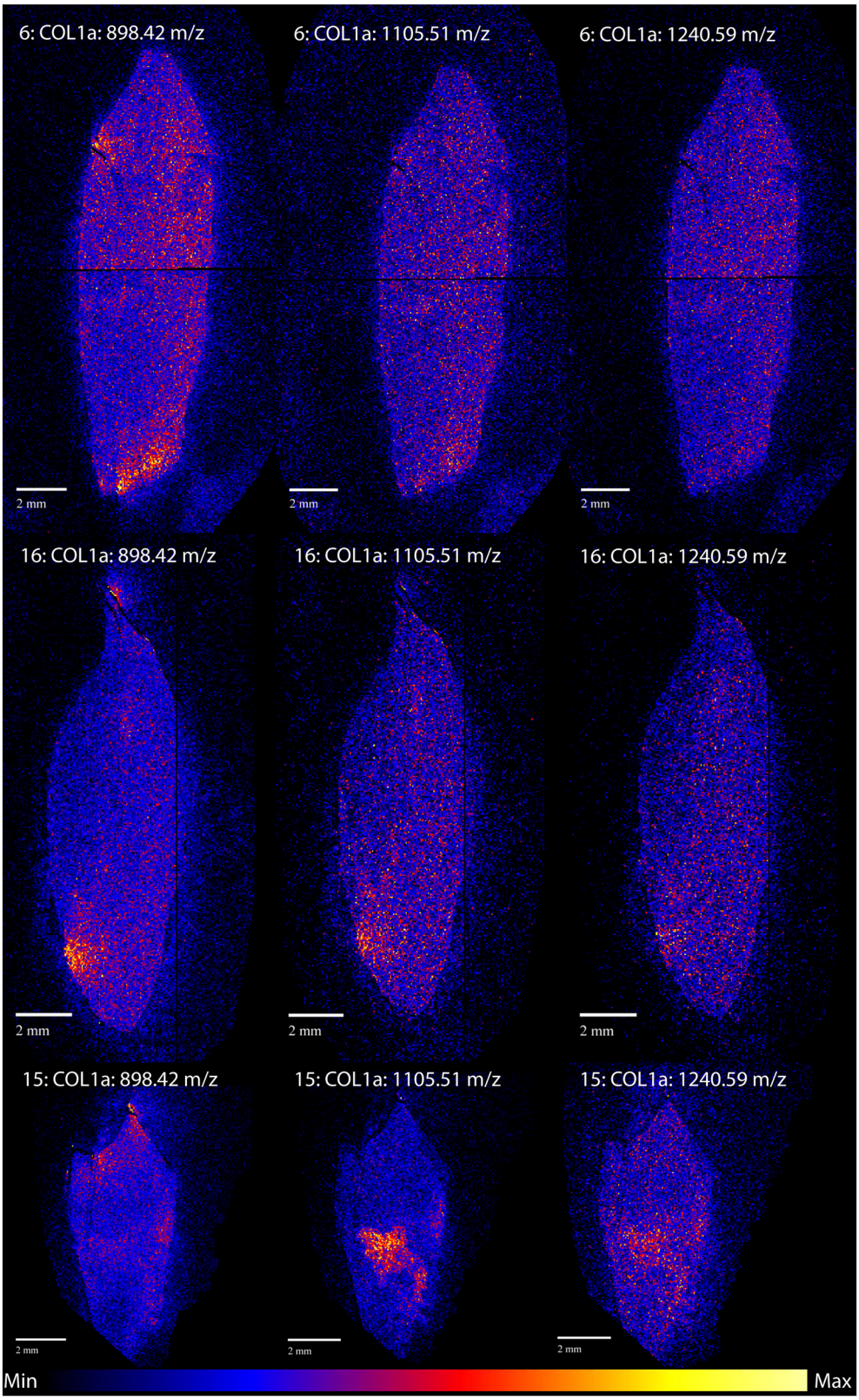

FIGURE 2 Spatial distribution of selected collagen alpha-1 (I) (COL1a) peptides for archaeological teeth numbers 6, 15 and 16. The figures represent a heatmap of the intensity of the selected peptides, with the brighter colours indicating increased intensity. Black indicates an intensity value of 0. The teeth are oriented with the crown to the top and the lingual side to the left [Color figure can be viewed at wileyonlinelibrary.com]

not align well with our images, but it is not clear how comparable these methods are to MSI.

Second, we expected the spatial distribution of proteins to align with the different tissue types within the tooth as previous studies had been able to distinguish between enamel, dentine and dental pulp with MSI.[22] For example, as the dental pulp cavity contains blood vessels during life, it was expected that haemoglobin might be concentrated around the pulp cavity. Instead the spatial distribution appears relatively homogeneous. In general we observe that peptides with high *m/z* values display more homogenous and less clear spatial

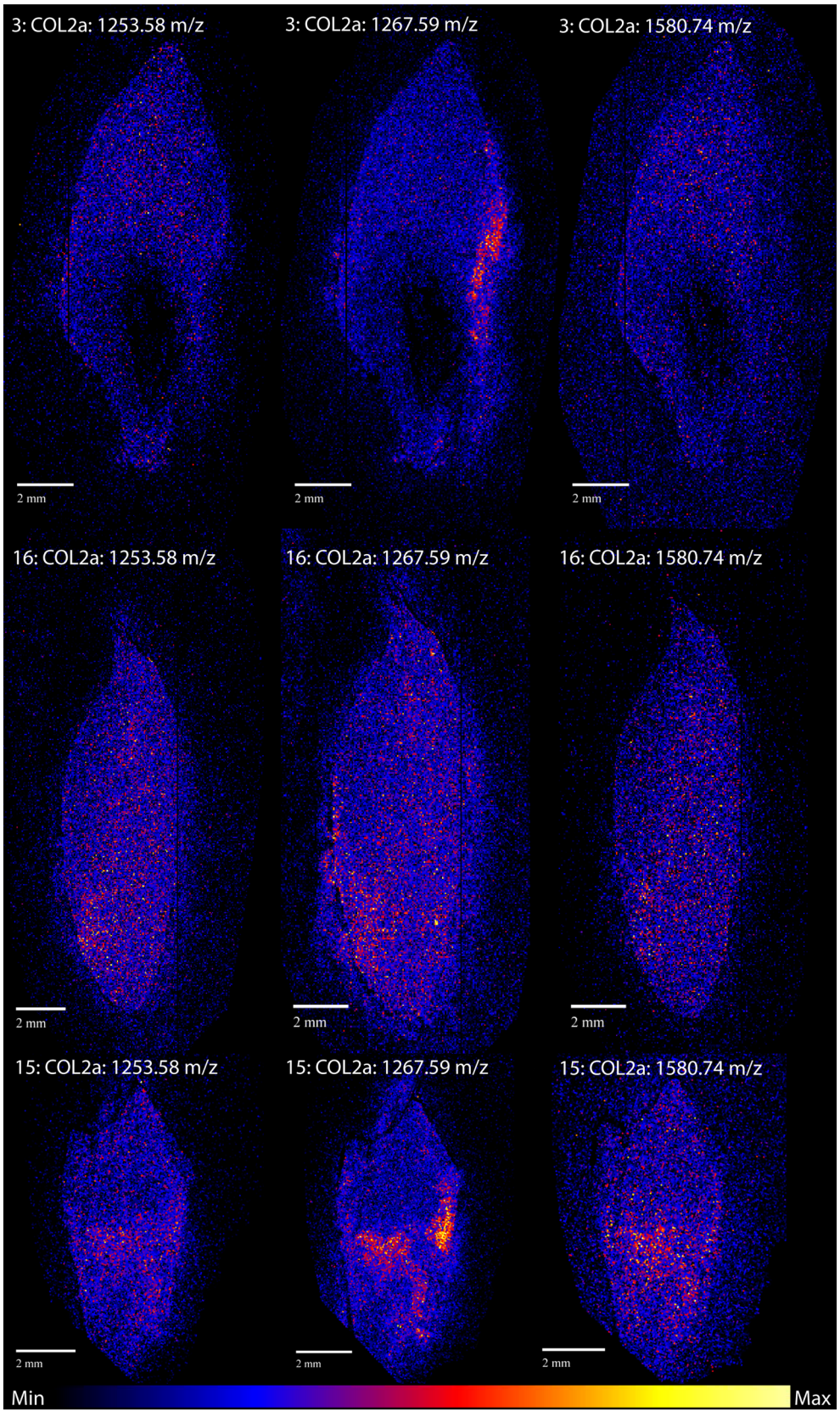

FIGURE 3 Spatial distribution of the collagen alpha-2 (I) (COL2a) peptides of teeth 3, 15 and 16. Sample 3 is oriented with the crown upwards and the lingual side to the right. Samples 15 and 16 are oriented with the crown to the top and the lingual side to the left [Color figure can be viewed at wileyonlinelibrary.com]

patterns, and therefore considering that the haemoglobin peptides have relatively large *m/z* values compared to the collagen alpha-1 (I), alpha-2-HS-glycoprotein and myosin light polypeptide 6 peptides, this might explain why the spatial pattern of haemoglobin appears to be much fainter. When examining this MSI data alone, this lack of correlation between protein function and tooth internal structure,

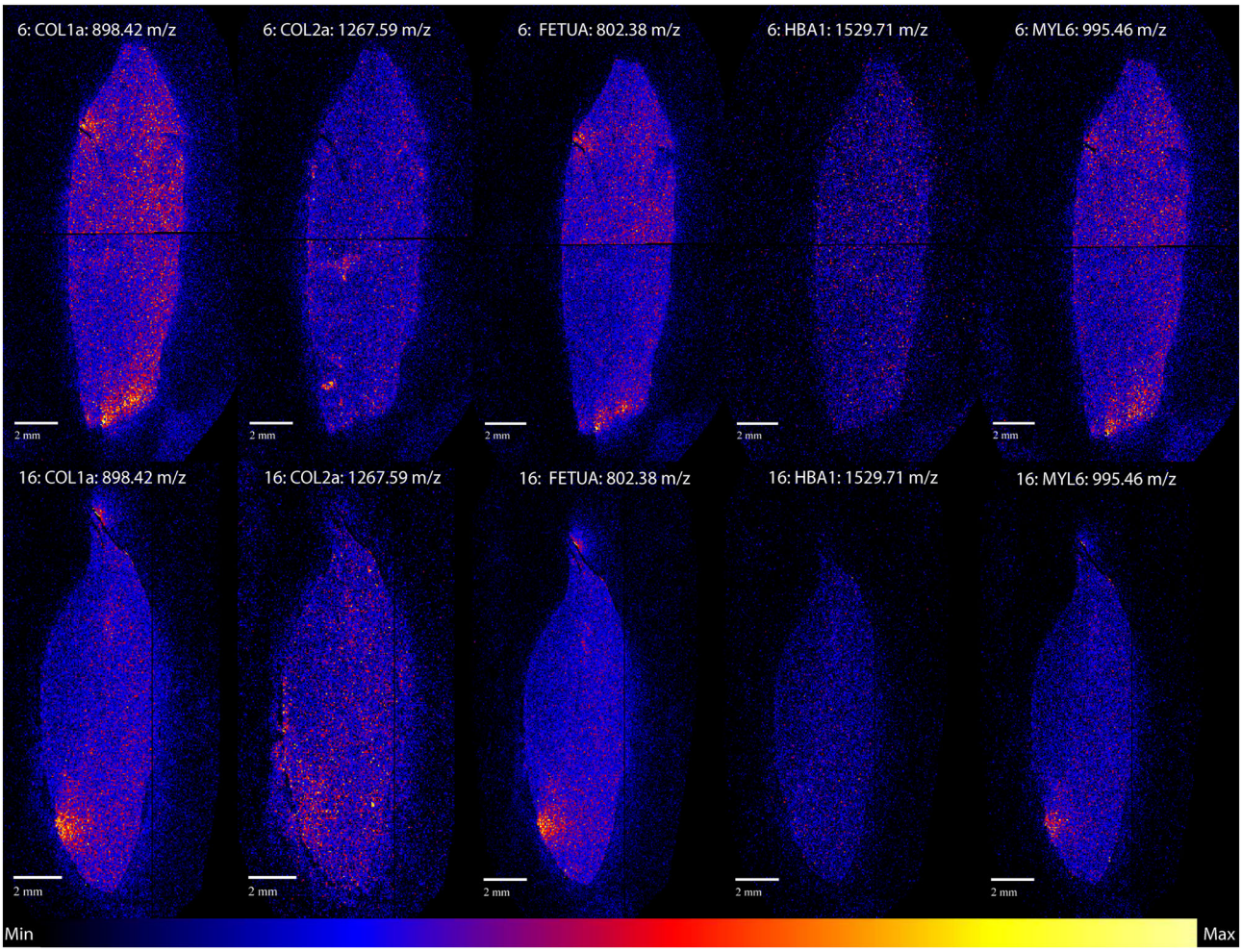

FIGURE 4 Spatial distribution of collagen alpha-1 (COL1a), collagen alpha-2 (COL2a), alpha-2-HS-glycoprotein (FETUA), haemoglobin subunit alpha (HBA1) and myosin light polypeptide 6 (MYL6) peptides for teeth 6 and 16. The teeth are orientated with their crowns up and the lingual side to the left [Color figure can be viewed at wileyonlinelibrary.com]

combined with similarities in spatial distribution between most of the selected proteins, suggests that the spatial distribution of a protein is not primarily guided by its function. A correlation between common bone proteins such as collagens and alpha-HS-glycoprotein was expected, but myosin and haemoglobin are primarily associated with muscles and blood, respectively.

Additionally, we hypothesised that after the internal structure, growth lines would be one of the main factors influencing protein distribution. The incremental growth pattern of teeth can be clearly visualised microscopically[76] and considering the little to no remodelling dentine experiences,[35,36,77] we would expect any influence of life history events on the abundance of proteins to manifest along the growth lines. Particularly in samples from individuals who showed LEH, which is a stress-caused disruption of enamel deposition, we had expected to see a change in protein distribution in the area of the tooth that was in development at the time of LEH formation. Instead of aligning either with structural differences or the growth line pattern, most peptides display either a 'hot-spot' (e.g., Figure 4, COL1a) pattern or appear relatively homogeneously distributed across the tooth (e.g., Figure 4, HBA1). In the 'hot-spot' pattern there are one or two hot spots of high intensity, frequently occurring close to the tooth's edge or a fracture in the section, although there is variation in the hot spot's exact location. The size of the hot spots varies considerably between teeth, although in general it is relatively small. It is possible that a relatively higher availability of denatured or degraded protein near the edges or fractures in the section may have contributed to the occurrence of hot spots at these locations. Trypsin's digestion efficiency is higher for denatured proteins and since the edges will have been more exposed to acid during the demineralisation and fractures indicate locations of reduced structural integrity this may have been a factor.

A few samples also contained extremely small areas of high intensities, which were observed in the images as bright white pixels. In some cases these even appeared to be located outside the tooth. We suspect that these minute areas of extreme high intensity are an artefact of the sample preparation, rather than areas that were significantly better protected from diagenetic damage or being caused by some biological phenomenon. However, in general the intensity

differences between these regions of extreme intensity and the rest of the tooth decrease significantly in the heavier peptides. It might be that these heavier peptides are better suited to show spatial differences in preservation because they dampen the effects of artefacts created during the analysis process.

4.1 | Sectioning and demineralisation

One explanation for our observed results might be that the observed patterns are an artefact of our methodology. Tissue sectioning is a critical step in the MSI workflow, with any imperfections, such as tears, fractures or fraying of the section, leading to missing or misrepresentative data. Indeed in this study we experienced a number of challenges with sampling that may have impacted on these results. Bone and teeth are most likely the two tissues most suited to the archaeological application of MSI, but these calcified tissues are notoriously difficult to section and often shatter on sectioning without a preparation protocol.[46] One reason for the difficulty in sectioning bone is that it consists of tissues of different hardness and breaks in the section are especially frequent at the transition between the different tissues.[49] The shattering of teeth on sectioning can be prevented by decalcifying the samples, an approach taken in this experiment, but during sectioning in this study we observed that variation in the hardness of the demineralised tissue resulted in tears in the section, rendering some sections unsuitable for analysis.

It can be difficult to estimate if a tooth has been completely demineralised based on a visual assessment alone. In addition, the enamel crown prevents the inspection of the underlying dentine, and the enamel and dentine often demineralise at different rates. Prolonged demineralisation was observed to dissolve the enamel, removing the possibility of analysing the spatial distribution of any enamel proteins, which, although they were not targeted in this analysis, could be useful to identify in future studies. Demineralisation also has the potential to disturb the distribution of biomolecules and potentially introduce contamination.[46,78] There have been no comparative studies between the use of decalcified and calcified tissues in MSI, making it difficult to estimate the scale of any potential disturbance caused by demineralisation. On the other hand, a disadvantage of leaving the tissue calcified is that the mineral component can prevent the biomolecules encased therein from ionising.[22] Our primary reasons for deciding to decalcify our samples in this study were to increase the ease of sectioning and the detectability of the targeted proteins. The risk of a potentially mildly disturbed protein distribution was deemed lower than the risk of not being able to acquire sections of sufficient quality and not detecting our target proteins. Detectability is especially an issue for noncollagenous proteins, as these proteins occur in much lower abundances than collagen.

Even after demineralisation, the risk of tearing and crumbling of the thin sections is still present and only a minority of thin sections is suitable for MSI analysis. A way to improve the sectioning process might be to cut the tooth in half along the root–crown axis and to embed it lying flat on its cut side. The other half may then be used for histological analysis. Histological analysis can aid in visualising the structure of the tissue, but the traditional process to produce histology thin sections is incompatible with the protocol for MSI thin sections. Histological sections on bone are often made from thicker sections that are ground down,[79] and grinding or polishing might result in smearing of the proteins. However, histology and MSI can be applied on the same slides[67,80] and this would be a valuable addition to any further MSI studies on teeth.

Lastly, a more minor issue is presented by the size of the teeth. For some of the larger teeth it was not possible to analyse the entire tooth in one acquisition. In general, it seems having two acquisitions for one tooth does not seem to present much of an issue. However, it may lead to some differences in overall intensity and thus the scaling of the heatmap, as probably happened for alpha-2-HS-glycoprotein in sample 6 (Figure 4).

4.2 | Authenticating the MSI identifications

In the workflow of this study we identified target peptides of interest from LC–MS/MS data, preceding their identification using MALDI-MSI. However, due to the mass window of MALDI-MSI, some of these peptides have the potential to be misidentified as one *m/z* could reflect more than one peptide within the mass window. MSI processing software may fail to distinguish these peptides of similar *m/z*. For example, we note that the peptides *m/z* 1660.78 (from haemoglobin subunit alpha) could be identified as other peptides from other proteins as they have a neutral mass difference smaller than the *m/z* window. We also note that in our study the majority of target peptides can confidently be assigned via MSI as the *m/z* is distinct from other potential peptides. Figure 5 groups the target peptides together based on the potential risk of interference from other peptides. We advise careful consideration of target peptides given the *m/z* window of MSI and caution in interpreting *m/z* which cannot confidently be assigned to a single peptide.

	Group 1 No doubt regarding authenticity	Group 2 Likely negligible distortion	Group 3 Likely limited distortion	Group 4 Potentially distorted
COL1a	898.51 1105.58		1240.68	
COL2a	1253.65	1267.68 1580.77		
FETUA	802.36		1226.68	
HBA1	1529.74			1660.78
MYL6	995.59		1532.62	1354.73

FIGURE 5 Grouping of the target peptides by their expected authenticity based on the *m/z* differences between the target peptides and other observed peptides. The peptides are denoted by the *m/z* of their [M + H] ion

4.3 | Implications and future research

Our results unequivocally show a heterogeneous distribution of collagen alpha-1 (I) and -2 (I), alpha-2-HS-glycoprotein and myosin light polypeptide 6 in the modern and archaeological teeth in this study, which we suspect represents intratooth variation in protein detection. Considering the similarities in spatial distribution between the selected proteins, we suspect that this pattern extends to other common bone proteins as well. Our current understanding of the observed patterns is insufficient to provide a comprehensive explanation of their causes or any physiological consequences of such a protein distribution. Nonetheless several implications are clear. It cannot be assumed that any single sample of a tooth accurately represents the relative protein abundance within the whole tooth. In addition, the fact that protein distribution does not appear to follow the growth pattern of teeth raises doubts regarding the possibility of correlating intratooth differences in protein abundance or composition with life history events, without further work to refine the MSI methods presented in this study.

MSI analysis on archaeological remains is ripe for further development, as here we demonstrate that MSI indeed delivers high resolution images of protein spatial distribution in archaeological remains, although interpreting these results is at present rather open-ended. Two areas of further technical development are quantified spatial analysis and a combined approach of histology and MSI, already discussed above. The analysis of the MSI images in this study has been mostly descriptive and relative. This serves the purpose of an initial examination of the protein distribution in teeth well, but it is limited in its explanatory power. Minor, yet potentially significant, differences in spatial distribution can easily become subjective if only discussed through visual inspection. The development of an appropriate and biologically meaningful statistical method for analysing intratooth differences in protein distribution was beyond the scope of this study, but it is clear to us that this should be the next step. Indeed, several statistical methods, both supervised and unsupervised, have been proposed,[55] but currently there is no standardised approach. For archaeological applications, we believe that future MSI studies could be fruitfully applied to identifying proteins and proteome variation in archaeological biological tissues, but also identifying protein distributions in other artefact classes, such as material culture objects, to yield rich insights into past protein preservation.

5 | CONCLUSION

In this study we have visualised the spatial distribution of proteins in archaeological biological remains using mass spectrometry imaging for the first time. The combined analysis of LC–MS/MS and MSI shows that in both modern and archaeological material, for example, collagen alpha-1(I) and -2 (I), alpha-2-HS-glycoprotein and myosin light polypeptide 6, have a heterogeneous intratooth spatial distribution, while haemoglobin subunit alpha appears to be homogeneously distributed. However, our hypotheses on the distribution of ancient proteins within the teeth, such as that proteins would reflect dental tissue type and would follow growth patterns, were largely not met, and we believe this could be due to challenges in protein detection and sample preparation. In trialling this method for the first time, we have also articulated a number of technical caveats and suggestions that we hope will be helpful to future researchers employing this emerging methodology. Nonetheless, our results show the value of MSI for revealing spatial patterns in protein distribution, and further development and application has the potential to be of immense benefit to our understanding of the nature and variation of ancient protein preservation in archaeological substrates.

ACKNOWLEDGMENTS

The study was supported by a University of York Research Priming Fund awarded to J.H., J.D., T.L. and P.G., and a Philip Leverhulme Prize awarded to J.H by the Leverhulme Trust. We thank the Bioscience Technology Facility and Chemistry Department at the University of York for mass spectrometry access and support. The instrumentation is part of the York Centre of Excellence in Mass Spectrometry. The centre was created thanks to a major capital investment through Science City York, supported by Yorkshire Forward with funds from the Northern Way Initiative and subsequent support from EPSRC (EP/K039660/1; EP/M028127/1). M.S. is funded by the Nederlandse Organisatie voor Wetenschapellijk Onderzoek (NWO) Neandertal Legacy award (VI.C.191.07). We would also like to thank the Gemeente Arnhem and its community for the opportunity to include samples from its past inhabitants in this study. Additionally, we are grateful to the anonymous donors of the modern samples for their participation.

DATA AVAILABILITY STATEMENT

The data that support the findings of this study are openly available on ProteomeXchange Consortium via the PRIDE partner repository at https://doi.org/10.6019/PXD038114.

PEER REVIEW

The peer review history for this article is available at https://publons.com/publon/10.1002/rcm.9486.

ORCID

Joannes Dekker https://orcid.org/0000-0002-3952-4448

REFERENCES

1. Welker F, Collins MJ, Thomas JA, et al. Ancient proteins resolve the evolutionary history of Darwin's south American ungulates. *Nature*. 2015;522(7554):81-84. doi:10.1038/nature14249
2. Hill RC, Wither MJ, Nemkov T, et al. Preserved proteins from extinct *Bison latifrons* identified by tandem mass spectrometry; Hydroxylysine glycosides are a common feature of ancient collagen. *Mol Cell Proteomics*. 2015;14(7):1946-1958. doi:10.1074/mcp.M114.047787
3. Welker F, Ramos-Madrigal J, Kuhlwilm M, et al. Enamel proteome shows that Gigantopithecus was an early diverging pongine. *Nature*. 2019;576(7786):262-265. doi:10.1038/s41586-019-1728-8

4. Buckley M, Recabarren OP, Lawless C, García N, Pino M. A molecular phylogeny of the extinct south American gomphothere through collagen sequence analysis. *Quat Sci Rev*. 2019;224:105882. doi:10.1016/j.quascirev.2019.105882
5. Harvey VL, LeFebvre MJ, de France SD, et al. Preserved collagen reveals species identity in archaeological marine turtle bones from Caribbean and Florida sites. *R Soc Open Sci*. 2019;6(10):191137. doi:10.1098/rsos.191137
6. Harvey VL, Keating JN, Buckley M. Phylogenetic analyses of ray-finned fishes (Actinopterygii) using collagen type I protein sequences. *R Soc Open Sci*. 2021;8(8):201955. doi:10.1098/rsos.201955
7. Peters C, Richter KK, Manne T, et al. Species identification of Australian marsupials using collagen fingerprinting. *R Soc Open Sci*. 2021;8(10):211229. doi:10.1098/rsos.211229
8. Procopio N, Chamberlain AT, Buckley M. Exploring biological and geological age-related changes through variations in intra- and intertooth proteomes of ancient dentine. *J Proteome Res*. 2018;17(3):1000-1013. doi:10.1021/acs.jproteome.7b00648
9. Parker GJ, Yip JM, Eerkens JW, et al. Sex estimation using sexually dimorphic amelogenin protein fragments in human enamel. *J Archaeol Sci*. 2019;101:169-180. doi:10.1016/j.jas.2018.08.011
10. Barbieri R, Mekni R, Levasseur A, et al. Paleoproteomics of the dental pulp: The plague paradigm. *PLoS ONE*. 2017;12(7):e0180552. doi:10.1371/journal.pone.0180552
11. Cleland TP, Sarancha JJ, France CAM. Proteomic profile of bone "collagen" extracted for stable isotopes: Implications for bulk and single amino acid analyses. *Rapid Commun Mass Spectrom*. 2021;35(6):e9025. doi:10.1002/rcm.9025
12. Gatti L, Lugli F, Sciutto G, et al. Combining elemental and immunochemical analyses to characterize diagenetic alteration patterns in ancient skeletal remains. *Sci Rep*. 2022;12(1):5112. doi:10.1038/s41598-022-08979-3
13. Procopio N, Chamberlain AT, Buckley M. Intra- and interskeletal proteome variations in fresh and buried bones. *J Proteome Res*. 2017;16(5):2016-2029. doi:10.1021/acs.jproteome.6b01070
14. Kendall C, Eriksen AMH, Kontopoulos I, Collins MJ, Turner-Walker G. Diagenesis of archaeological bone and tooth. *Palaeogeogr Palaeoclimatol Palaeoecol*. 2018;491:21-37. doi:10.1016/j.palaeo.2017.11.041
15. Jágr M, Eckhardt A, Pataridis S, Broukal Z, Dušková J, Mikšík I. Proteomics of human teeth and saliva. *Physiol Res*. 2014;63(Suppl 1):S141-S154. doi:10.33549/physiolres.932702
16. Eckhardt A, Jágr M, Pataridis S, Mikšík I. Proteomic analysis of human tooth pulp: Proteomics of human tooth. *J Endod*. 2014;40(12):1961-1966. doi:10.1016/j.joen.2014.07.001
17. Jágr M, Ergang P, Pataridis S, Kolrosová M, Bartoš M, Mikšík I. Proteomic analysis of dentin-enamel junction and adjacent protein-containing enamel matrix layer of healthy human molar teeth. *Eur J Oral Sci*. 2019;127(2):112-121. doi:10.1111/eos.12594
18. Green DR, Schulte F, Lee KH, Pugach MK, Hardt M, Bidlack FB. Mapping the tooth enamel proteome and amelogenin phosphorylation onto mineralizing porcine tooth crowns. *Front Physiol*. 2019;10:925. doi:10.3389/fphys.2019.00925
19. Sharma V, Srinivasan A, Roychoudhury A, et al. Publisher correction: Characterization of protein extracts from different types of human teeth and insight in biomineralization. *Sci Rep*. 2019;9(1):17517. doi:10.1038/s41598-019-53780-4
20. Malik Z, Alexiou M, Hallgrimsson B, Economides AN, Luder HU, Graf D. Bone morphogenetic protein 2 coordinates early tooth mineralization. *J Dent Res*. 2018;97(7):835-843. doi:10.1177/0022034518758044
21. Giovani PA, Martins L, Salmon CR, et al. Comparative proteomic analysis of dental cementum from deciduous and permanent teeth. *J Periodontal Res*. 2021;56(1):173-185. doi:10.1111/jre.12808
22. Hirano H, Masaki N, Hayasaka T, et al. Matrix-assisted laser desorption/ionization imaging mass spectrometry revealed traces of dental problem associated with dental structure. *Anal Bioanal Chem*. 2014;406(5):1355-1363. doi:10.1007/s00216-013-7075-y
23. Czermak A, Schermelleh L, Lee-Thorp J. Fluorescence screening of collagen preservation in tooth dentine. *Palaeogeogr Palaeoclimatol Palaeoecol*. 2019;532:109249. doi:10.1016/j.palaeo.2019.109249
24. Mitsiadis TA, Filatova A, Papaccio G, Goldberg M, About I, Papagerakis P. Distribution of the amelogenin protein in developing, injured and carious human teeth. *Front Physiol*. 2014;5:477. doi:10.3389/fphys.2014.00477
25. Beaumont J, Montgomery J, Buckberry J, Jay M. Infant mortality and isotopic complexity: New approaches to stress, maternal health, and weaning. *Am J Phys Anthropol*. 2015;157(3):441-457. doi:10.1002/ajpa.22736
26. Smith TM, Austin C, Green DR, et al. Wintertime stress, nursing, and lead exposure in Neanderthal children. *Sci Adv*. 2018;4(10):eaau9483. doi:10.1126/sciadv.aau9483
27. Britton K, Grimes V, Dau J, Richards MP. Reconstructing faunal migrations using intra-tooth sampling and strontium and oxygen isotope analyses: A case study of modern caribou (*Rangifer tarandus granti*). *J Archaeol Sci*. 2009;36(5):1163-1172. doi:10.1016/j.jas.2009.01.003
28. Dean MC, Scandrett AE. Rates of dentine mineralization in permanent human teeth. *Int J Osteoarchaeol*. 1995;5(4):349-358. doi:10.1002/oa.1390050405
29. Eerkens JW, Berget AG, Bartelink EJ. Estimating weaning and early childhood diet from serial micro-samples of dentin collagen. *J Archaeol Sci*. 2011;38(11):3101-3111. doi:10.1016/j.jas.2011.07.010
30. Tian X, Zhu C, Shui T, Huang Y. Diets, eco-environments and seasonal variations recorded in the oxygen and carbon isotopic compositions of mammal tooth enamel from the Shunshanji site, Sihong County, Jiangsu Province, China. *Chin Sci Bull*. 2013;58(31):3788-3795. doi:10.1007/s11434-013-5894-z
31. Beaumont J, Montgomery J. Oral histories: A simple method of assigning chronological age to isotopic values from human dentine collagen. *Ann Hum Biol*. 2015;42(4):407-414. doi:10.3109/03014460.2015.1045027
32. Temple DH. Bioarchaeological evidence for adaptive plasticity and constraint: Exploring life-history trade-offs in the human past. *Evol Anthropol*. 2019;28(1):34-46. doi:10.1002/evan.21754
33. Dąbrowski, Kulus, Grzelak. Assessing weaning stress–relations between enamel hypoplasia, δ18O and δ13C values in human teeth obtained from early modern cemeteries in Wroclaw …. *Ann Anat*Published online. 2020. https://www.sciencedirect.com/science/article/pii/S094096022030090X
34. Beaumont J, Gledhill A, Lee-Thorp J, Montgomery J. Childhood diet: A closer examination of the evidence from dental tissues using stable isotope analysis of incremental human dentine. *Archaeometry*. 2013;55(2):277-295. doi:10.1111/j.1475-4754.2012.00682.x
35. Burt NM, Garvie-Lok S. A new method of dentine microsampling of deciduous teeth for stable isotope ratio analysis. *J Archaeol Sci*. 2013;40(11):3854-3864. doi:10.1016/j.jas.2013.05.022
36. Czermak A, Schermelleh L, Lee-Thorp J. Imaging-assisted time-resolved dentine sampling to track weaning histories. *Int J Osteoarchaeol*. 2018;28(5):535-541. doi:10.1002/oa.2697
37. Czermak A, Fernández-Crespo T, Ditchfield PW, Lee-Thorp JA. A guide for an anatomically sensitive dentine microsampling and age-alignment approach for human teeth isotopic sequences. *Am J Phys Anthropol*. 2020;173(4):776-783. doi:10.1002/ajpa.24126
38. Cheung C, Fernández-Crespo T, Mion L, et al. Micro-punches vs. micro-slices for serial sampling of human dentine: Striking a balance between improved temporal resolution and measuring

additional isotope systems. *Rapid Commun Mass Spectrom*. 2022; 36(21):e9380. doi:10.1002/rcm.9380
39. Amstalden van Hove ER, Smith DF, Heeren RMA. A concise review of mass spectrometry imaging. *J Chromatogr A*. 2010;1217(25):3946-3954. doi:10.1016/j.chroma.2010.01.033
40. Cillero-Pastor B, Heeren RMA. Matrix-assisted laser desorption ionization mass spectrometry imaging for peptide and protein analyses: A critical review of on-tissue digestion. *J Proteome Res*. 2014;13(2):325-335. doi:10.1021/pr400743a
41. Mascini NE, Heeren RMA. Protein identification in mass-spectrometry imaging. *Trends Anal Chem*. 2012;40:28-37. doi:10.1016/j.trac.2012.06.008
42. Schulz S, Becker M, Groseclose MR, Schadt S, Hopf C. Advanced MALDI mass spectrometry imaging in pharmaceutical research and drug development. *Curr Opin Biotechnol*. 2019;55:51-59. doi:10.1016/j.copbio.2018.08.003
43. Cuypers E, Claes BSR, Biemans R, et al. "On the spot" digital pathology of breast cancer based on single-cell mass spectrometry imaging. *Anal Chem*. 2022;94(16):6180-6190. doi:10.1021/acs.analchem.1c05238
44. Taylor MJ, Lukowski JK, Anderton CR. Spatially resolved mass spectrometry at the single cell: Recent innovations in proteomics and metabolomics. *J Am Soc Mass Spectrom*. 2021;32(4):872-894. doi:10.1021/jasms.0c00439
45. Colley M, Liang S, Tan C, Trobough KP, Bach SBH, Chun YHP. Mapping and identification of native proteins of developing teeth in mouse mandibles. *Anal Chem*. 2020;92(11):7630-7637. doi:10.1021/acs.analchem.0c00359
46. Vandenbosch M, Nauta SP, Svirkova A, et al. Sample preparation of bone tissue for MALDI-MSI for forensic and (pre)clinical applications. *Anal Bioanal Chem*. 2021;413(10):2683-2694. doi:10.1007/s00216-020-02920-1
47. Svirkova A, Turyanskaya A, Perneczky L, Streli C, Marchetti-Deschmann M. Multimodal imaging of undecalcified tissue sections by MALDI MS and μXRF. *Analyst*. 2018;143(11):2587-2595. doi:10.1039/c8an00313k
48. Seeley EH, Wilson KJ, Yankeelov TE, et al. Co-registration of multi-modality imaging allows for comprehensive analysis of tumor-induced bone disease. *Bone*. 2014;61:208-216. doi:10.1016/j.bone.2014.01.017
49. Schaepe K, Bhandari DR, Werner J, et al. Imaging of lipids in native human bone sections using TOF-secondary ion mass spectrometry, atmospheric pressure scanning microprobe matrix-assisted laser desorption/ionization Orbitrap mass spectrometry, and Orbitrap-secondary ion mass spectrometry. *Anal Chem*. 2018;90(15):8856-8864. doi:10.1021/acs.analchem.8b00892
50. Kramell AE, García-Altares M, Pötsch M, et al. Mapping natural dyes in archeological textiles by imaging mass spectrometry. *Sci Rep*. 2019; 9(1):2331. doi:10.1038/s41598-019-38706-4
51. Hammann S, Scurr DJ, Alexander MR, Cramp LJE. Mechanisms of lipid preservation in archaeological clay ceramics revealed by mass spectrometry imaging. *Proc Natl Acad Sci U S a*. 2020;117(26):14688-14693. doi:10.1073/pnas.1922445117
52. Atrei A, Benetti F, Gliozzo E, Perra G, Marchettini N. Chemical characterization of protein based binders in painting samples by means of ToF-SIMS: Tests on ancient and model samples. *Int J Mass Spectrom*. 2014;369:9-15. doi:10.1016/j.ijms.2014.05.001
53. Tian H, Seracini M, Schimmel K, Benkovic SJ, Winograd N. SIMS (imaging secondary ion mass spectrometry) analysis of a cross-section sample from Leonardo da Vinci's adoration of the magi. *Res Sq*. Published online October 29. 2020. doi:10.21203/rs.3.rs-97371/v1
54. Mazel V, Richardin P, Debois D, et al. The patinas of the Dogon–Tellem statuary: A new vision through physico-chemical analyses. *J Cult Herit*. 2008;9(3):347-353. doi:10.1016/j.culher.2007.11.003
55. Buchberger AR, DeLaney K, Johnson J, Li L. Mass spectrometry imaging: A review of emerging advancements and future insights. *Anal Chem*. 2018;90(1):240-265. doi:10.1021/acs.analchem.7b04733
56. Cleland TP, Schroeter ER. A comparison of common mass spectrometry approaches for Paleoproteomics. *J Proteome Res*. 2018; 17(3):936-945. doi:10.1021/acs.jproteome.7b00703
57. Kaya I, Jennische E, Lange S, Malmberg P. Multimodal chemical imaging of a single brain tissue section using ToF-SIMS, MALDI-ToF and immuno/histochemical staining. *Analyst*. 2021;146(4):1169-1177. doi:10.1039/d0an02172e
58. Widbiller M, Schweikl H, Bruckmann A, et al. Shotgun proteomics of human dentin with different prefractionation methods. *Sci Rep*. 2019; 9(1):4457. doi:10.1038/s41598-019-41144-x
59. Zielman G, Baetsen WA. *Wat de Nieuwe Sint Jansbeek Boven Water Bracht: Dood En Leven in Het Arnhemse Verleden: Archeologisch Onderzoek Sint Jansbeek Te Arnhem*. Vol. 4476. RAAP; 2020.
60. Buikstra U. Standards for data collection from human skeletal remains. *Arkansas Archaeol Survey Res Serie*. Published Online. 1994; 1994.
61. Scott AB, Choi KY, Mookherjee N, Hoppa RD, Larcombe LA. The biochemical signatures of stress: A preliminary analysis of osteocalcin concentrations and macroscopic skeletal changes associated with stress in the 13th–17th centuries black friars population. *Am J Phys Anthropol*. 2016;159(4):596-606. doi:10.1002/ajpa.22915
62. Ritzman TB, Baker BJ, Schwartz GT. A fine line: A comparison of methods for estimating ages of linear enamel hypoplasia formation. *Am J Phys Anthropol*. 2008;135(3):348-361. doi:10.1002/ajpa.20750
63. Schroeter ER, DeHart CJ, Schweitzer MH, Thomas PM, Kelleher NL. Bone protein "extractomics": Comparing the efficiency of bone protein extractions of *Gallus gallus* in tandem mass spectrometry, with an eye towards paleoproteomics. *PeerJ*. 2016;4:e2603. doi:10.7717/peerj.2603
64. Perez-Riverol Y, Bai J, Bandla C, et al. The PRIDE database resources in 2022: A hub for mass spectrometry-based proteomics evidences. *Nucleic Acids Res*. 2022;50(D1):D543-D552. doi:10.1093/nar/gkab1038
65. Wenger CD, Coon JJ. A proteomics search algorithm specifically designed for high-resolution tandem mass spectra. *J Proteome Res*. 2013;12(3):1377-1386. doi:10.1021/pr301024c
66. Solntsev SK, Shortreed MR, Frey BL, Smith LM. Enhanced global post-translational modification discovery with MetaMorpheus. *J Proteome Res*. 2018;17(5):1844-1851. doi:10.1021/acs.jproteome.7b00873
67. Fujino Y, Minamizaki T, Yoshioka H, Okada M, Yoshiko Y. Imaging and mapping of mouse bone using MALDI-imaging mass spectrometry. *Bone Rep*. 2016;5:280-285. doi:10.1016/j.bonr.2016.09.004
68. Veselkov K, Sleeman J, Claude E, et al. BASIS: High-performance bioinformatics platform for processing of large-scale mass spectrometry imaging data in chemically augmented histology. *Sci Rep*. 2018;8(1):4053. doi:10.1038/s41598-018-22499-z
69. Gurdeep Singh R, Tanca A, Palomba A, et al. Unipept 4.0: Functional analysis of Metaproteome data. *J Proteome Res*. 2019;18(2):606-615. doi:10.1021/acs.jproteome.8b00716
70. Buckley M, Collins M, Thomas-Oates J, Wilson JC. Species identification by analysis of bone collagen using matrix-assisted laser desorption/ionisation time-of-flight mass spectrometry. *Rapid Commun Mass Spectrom*. 2009;23(23):3843-3854. doi:10.1002/rcm.4316
71. Wadsworth C, Buckley M. Proteome degradation in fossils: Investigating the longevity of protein survival in ancient bone. *Rapid Commun Mass Spectrom*. 2014;28(6):605-615. doi:10.1002/rcm.6821
72. Sawafuji R, Cappellini E, Nagaoka T, et al. Proteomic profiling of archaeological human bone. *R Soc Open Sci*. 2017;4(6):161004. doi:10.1098/rsos.161004

73. Solazzo C, Fitzhugh WW, Rolando C, Tokarski C. Identification of protein remains in archaeological potsherds by proteomics. *Anal Chem*. 2008;80(12):4590-4597. doi:10.1021/ac800515v
74. Nielsen-Marsh CM, Richards MP, Hauschka PV, et al. Osteocalcin protein sequences of Neanderthals and modern primates. *Proc Natl Acad Sci U S A*. 2005;102(12):4409-4413. doi:10.1073/pnas.0500450102
75. Smith C, Voisin S, Al Saedi A, et al. Osteocalcin and its forms across the lifespan in adult men. *Bone*. 2020;130:115085. doi:10.1016/j.bone.2019.115085
76. Papakyrikos AM, Arora M, Austin C, et al. Biological clocks and incremental growth line formation in dentine. *J Anat*. 2020;237(2):367-378. doi:10.1111/joa.13198
77. Smith AJ, Scheven BA, Takahashi Y, Ferracane JL, Shelton RM, Cooper PR. Dentine as a bioactive extracellular matrix. *Arch Oral Biol*. 2012;57(2):109-121. doi:10.1016/j.archoralbio.2011.07.008
78. Khodjaniyazova S, Hanne NJ, Cole JH, Muddiman DC. Mass spectrometry imaging (MSI) of fresh bones using infrared matrix-assisted laser desorption electrospray ionization (IR-MALDESI). *Anal Methods*. 2019;11(46):5929-5938. doi:10.1039/c9ay01886g
79. Williamson RA. Histological preparation of teeth and tooth growth. *Oral Biol Dent*. 2015;3(1):3. doi:10.7243/2053-5775-3-3
80. Chaurand P, Schwartz SA, Billheimer D, Xu BJ, Crecelius A, Caprioli RM. Integrating histology and imaging mass spectrometry. *Anal Chem*. 2004;76(4):1145-1155. doi:10.1021/ac0351264

SUPPORTING INFORMATION

Additional supporting information can be found online in the Supporting Information section at the end of this article.

How to cite this article: Dekker J, Larson T, Tzvetkov J, et al. Spatial analysis of the ancient proteome of archeological teeth using mass spectrometry imaging. *Rapid Commun Mass Spectrom*. 2023;37(8):e9486. doi:10.1002/rcm.9486